Iraqi Journal of Scientific and Industrial Research
Volume 2, Issue (4), October-December 2023, pp. 83-90

Position Estimation of Sensorless Rotor in Permanent Magnet Synchronous Motor Drives Based on Hardware-In-Loop Simulator

Shavan J. MAKAROS

Department of Electronic Engineering, College of Engineering, University of Yerevan, Yerevan, ARMENIA

Abstract

The paper presents an investigation of field oriented control strategy of Permanent Magnet Synchronous Motor (PMSM) based on hardware in the loop simulation (HIL) over a wide speed range. A sensorless rotor position estimation using sliding mode observer for permanent magnet synchronous motor is illustrated considering the effects of magnetic saturation between the d and q axes. The cross saturation between d and q axes has been calculated by finite-element analysis. Therefore, the inductance measurement regards the saturation and cross saturation which are used to obtain the suitable id-characteristics in base and flux weakening regions. Real time matrix multiplication in Field Programmable Gate Array (FPGA) using floating point number system is used utilizing Quartus-II environment to develop FPGA designs and then download these designs files into development kit. dSPACE DS1103 is utilized for Pulse Width Modulation (PWM) switching and the controller. The hardware in the loop results conducted to that from the Matlab simulation. Various dynamic conditions have been investigated.

Keywords: Magnetic saturation, Rotor position estimation, Sliding mode observer, Hardware in the loop (HIL)

Received: 19 January 2023; **Revised:** 01 May 2023; **Accepted:** 08 May 2023; **Published:** 1 October 2023

1. Introduction

Permanent Magnet Synchronous Motors (PMSM) are mechanically robust for industry applications. Sensorless estimation has many advantages such as lower cost, reliability and robustness .The effective small air gap in these machines allow the control in the constant torque region as well as in the field-weakening constant power region up to high speed. There is cross-coupling between the direct and quadrature axes not only due to the inherent physical saliency, but also due to the effects of main-flux saturation which is called cross-saturation [1-7].

Many authors have been considered the inductance L_d and L_q were constants in the motor model but in actual conditions, the iron gets saturated results an increase in the magnetic flux. Hence, the saturation effect changes the inductance. Taking the saturation effect into consideration for machine modeling will improve the performance as well as reduce the estimation errors [8]. Some authors have been considering the magnetic saturation on position sensorless estimation drive.

Akitomo et al. [9] described the sensorless control based on the variation of the phase inductance with

respect to the rotor position and also the phase current, hence the magnetic saturation is affected by the phase current. They used the change of the slope of the phase inductance when the rotor and stator poles are aligned for a low speed range while the commutation angel is advanced based on the difference between the phase inductance at the aligned position and the one computed every sampling for a high speed range. However, proposed method can be applied within low and medium speed ranges.

In this paper a sliding mode observer (SMO) is used to estimate the rotor position including the effect of the cross saturation. Sliding mode observer is simple and more robust against the parameters variation, but it suffers from the chattering problem, however this problem can be solved by using a low pass filter [10-12]. A strong knowledge is required to analyze the influence of the magnetic saturation effects on the drive performance in base and flux weakening regions.

Hardware in the loop simulation offers the rapid prototyping by reducing time required for development and cost. A real time code generation interfaced to Matlab/Simulink is used to convert the control model and executed with dSPACE DS1103 for a suitable hardware circuit. However, a virtual motor interfaced with feedback signals of motor terminals currents as shown in Fig. (1). While simulation is running, dSPACE ControlDesk can observe many variables. This leads to visualize and adjust easily the control parameters saving time and cost indeed. A suitable sampling time is required when the drive reaches saturation level then a sufficient off time is required for de-flux current. Estimation for Sensorless control will not be accurate of a high speed range due to the high current ripple caused by the variation of inductance parameters $L_d(i_d,i_q)$ and $L_q(i_d,i_q)$ which also affected by the on and off switching actions. Moreover, the nonlinearity of the drive model gains an estimation error.

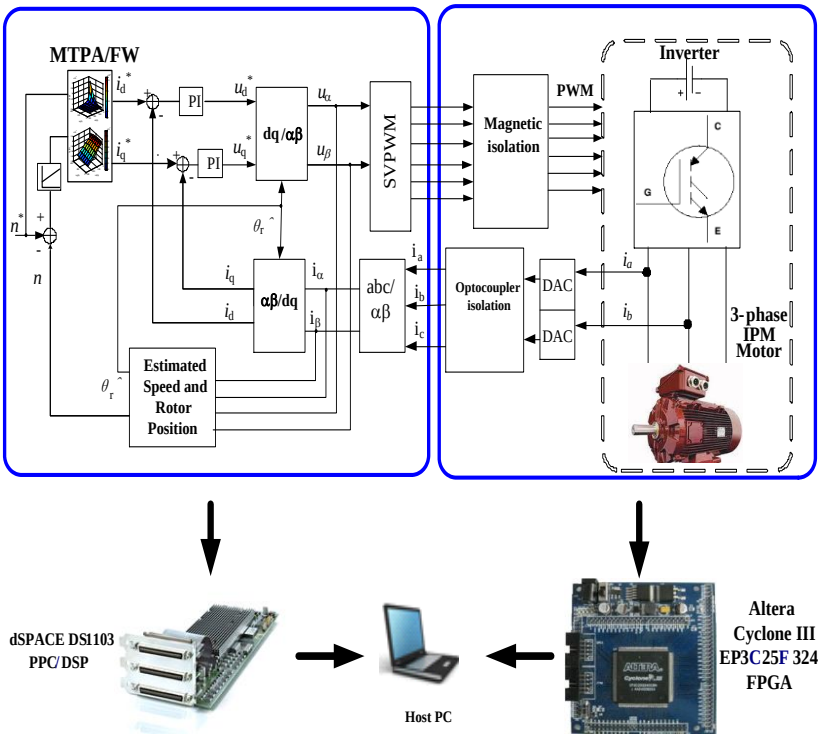

Fig. (1) Diagram of HIL simulator Sensorless System

2. PMSM Model

Neglecting the magnetic cross coupling between the orthogonal axes [12], then the simplest way to model the saturation as given in the equations below:

$$\left.\begin{aligned} u_{sd} &= R_s i_{sd} + \frac{d\psi_{sd}}{dt} - \omega_r \psi_{sq} \\ u_{sq} &= R_s i_{sq} + \frac{d\psi_{sq}}{dt} + \omega_r \psi_{sd} \end{aligned}\right\} \quad (1)$$

The magnetic flux linkages in d and q axes are $\psi_{sd}=L_{sd}\,i_{sd} + \psi_m$ and $\psi_{sq}=L_{sq}\,i_{sq}$. Substitute ψ_{sd} *and* ψ_{sq} into Eq. (1) gets the following matrix equation:

$$\begin{bmatrix} u_{sd} \\ u_{sq} \end{bmatrix} = \begin{bmatrix} R_s + \frac{dL_{sd}}{dt} & -\omega_r L_{sq} \\ \omega_r L_{sd} & R_s + \frac{dL_{sq}}{dt} \end{bmatrix} \begin{bmatrix} i_{sd} \\ i_{sq} \end{bmatrix} + \begin{bmatrix} 0 \\ \omega_r \psi_m \end{bmatrix} \quad (2)$$

The electromagnetic torque equation is given as in Eq. (3):

$$T_e = \frac{3}{2} np(\psi_m + (L_{sd} - L_{sq}) i_{sd}) i_{sq} \quad (3)$$

3. Saturation Effects and Inductance Calculation

The main issue effect on the sensorless control performance of PM machines is the cross saturation effect [13]. However, when the machine is loaded leads to misaligned of magnetic d-axis with respect to PM axis. Cross-saturation effect produces rotor position estimation errors which are based on inherent saliency.

Inductance calculation based on coupling and saturation without skew slot. Finite element models have been used to calculate the inductance variation as L_d and L_q are function with both i_d and i_q. However, no need finite element models by the controllers in the experiments in order to robust the system.

Figure (2) is obtained from the finite element method using Maxwell software package. From Fig. (2a) it can be noticed that L_d is quite large especially at higher values of i_q, i.e., it became greatly saturated. While in Fig. (2b) L_q is gradually decreased at higher values of i_d and i_q currents, therefore, it has a little effect.

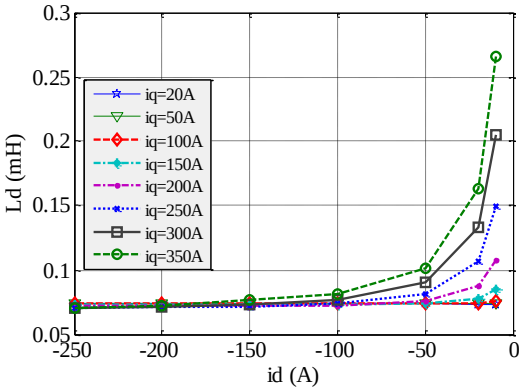

(a)

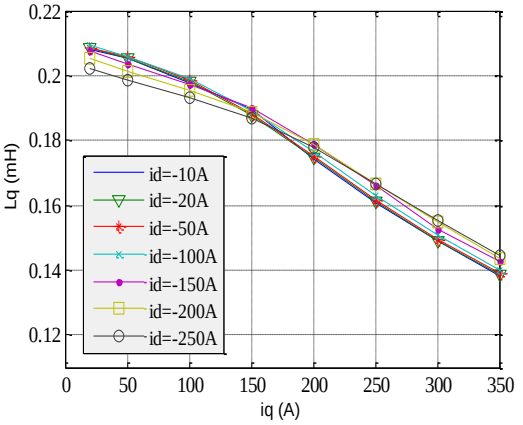

(b)

Fig. (2) Magnetic saturation (a) L_d (i_d,i_q), (b) L_q (i_d,i_q)

4. Sliding Mode Observer Design

The observer was designed depending on the motor model equations. Let the stator currents in □□ axis as $\bar{\imath}_{\alpha\beta} = \hat{\imath}_{\alpha\beta} - i_{\alpha\beta}$. The sliding mode occurs after a finite time interval $\bar{\imath}_\alpha = 0$ and $\bar{\imath}_\beta = 0$. By setting $\hat{\imath}_\alpha = 0$ and $\hat{\imath}_\beta = 0$, the back EMF will be

$$\begin{bmatrix} e_\alpha \\ e_\beta \end{bmatrix} = \begin{bmatrix} l_1 sign(\bar{i}_\alpha) \\ l_1 sign(\bar{i}_\beta) \end{bmatrix} \quad (4)$$

where l_1 is the observer constant and the subscript "^" indicates the estimated values

Equivalent control vector is Z_{eq}. The sliding mode slope depends on the value of the feedback gain, however at high speed l_1 is set to -0.9. The equivalent control Z_{eq} can be obtained by using a low pass filter (LPF) as given in Eq. (5) and it is shown in Fig. (3):

$$\begin{bmatrix} Z_{eq\alpha} \\ Z_{eq\beta} \end{bmatrix} = k \begin{bmatrix} sign(\hat{i}_\alpha - i_\alpha) \dfrac{\omega_c}{s+\omega_c} \\ sign(\hat{i}_\beta - i_\beta) \dfrac{\omega_c}{s+\omega_c} \end{bmatrix} \quad (5)$$

where ω_c is the cutoff frequency and k is normally positive

Consequently, the estimated rotor position angle can be obtained by using the equivalent control Z_{eq}, as:

$$\hat{\theta}_r = \tan^{-1}\left(\frac{-\hat{e}_\alpha}{\hat{e}_\beta}\right) = \tan^{-1}\left(\frac{-Z_{eq\alpha}}{Z_{eq\beta}}\right) \quad (6)$$

Noting that the estimated rotor position should be added to ω_r when the rotation is reversed. Therefore a compensation algorithm is required to adjust the accurate estimated rotor position.

The sliding mode observer motor model is modeled with the parameter variation of the L_d and L_q that is caused by the cross saturation. Thereafter, these affects will influence on the system performance due to the dependency on these parameters and also its influences on the currents and voltages used to estimate rotor position and speed. These effects will be discussed in simulation results section. Matlab/Simulink for sensorless control using SMO is shown in Fig. (4).

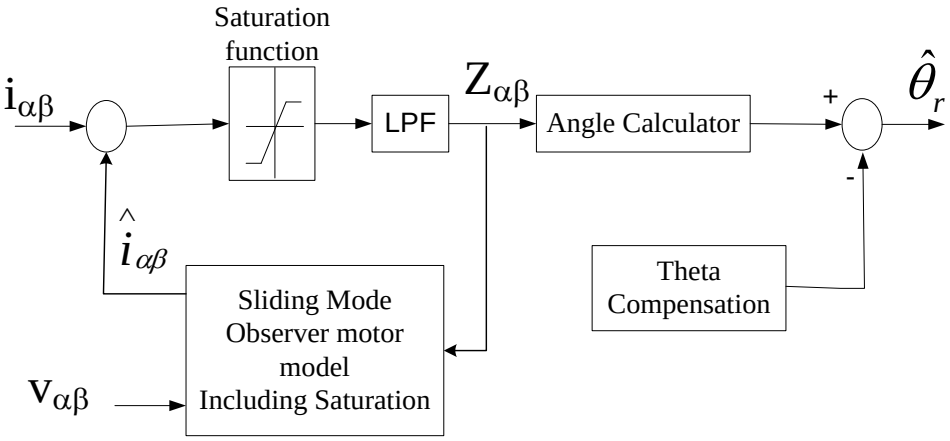

Fig. (3) Sliding mode observer model

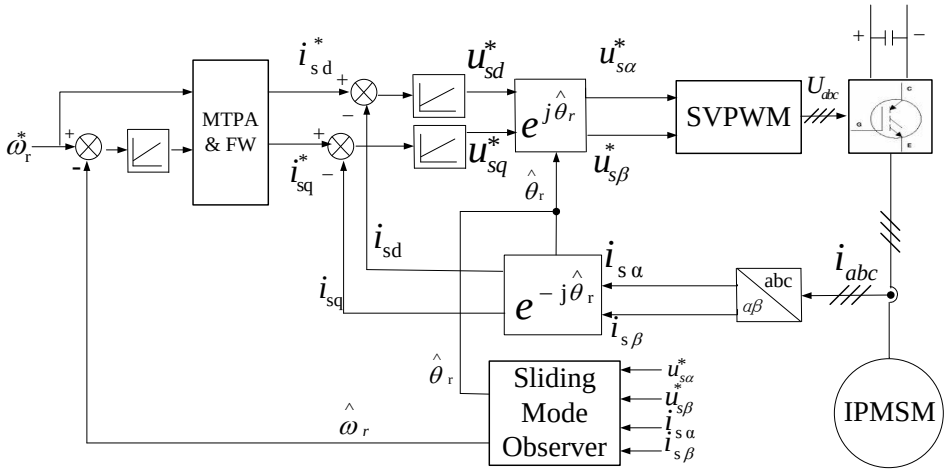

Fig. (4) Matlab block diagram with sliding mode observer

5. Simulation Results

Figure (5a) shows the i_d, i_q variation over a wide

speed range to verify the cross saturation, the i_d and i_q currents became distorted at high speed values due to the PI controller and parameter variations. Figure (5b) depicts the estimated rotor position including the effect of the cross saturation. It is clear that the rotor position cannot be estimated accurately at starting conditions because of zero voltages and currents. The simulation results do not illustrate the influence of cross saturation clearly as the sensorless rotor position estimation by sliding mode is robust with uncertainty parameters variation.

Figures (5c) and (5d) show i_d and variation under different values of speed beyond the base speed. When the sampling time is 10μs, the estimated angle will be advanced the actual angle, whilst when the sampling time is set to 1μs the error position between than actual and estimated may be quiet little, $Z_{\alpha\beta}$, $i_{\alpha\beta}$, $e_{\alpha\beta}$, $\hat{\theta}$ and θ illustrate the switching instants. For 1μs sampling time, the i_{abc} and $e_{\alpha\beta}$ reach saturation before the time off then a sufficient time off for de-flux current.

6. HIL Implementation

The test system platform is implemented with HIL includes dSPACE and FPGA platform. dSPACE DS1103 is used for model the controller and PWM. FPGA is utilized to model both the motor and inverter.

(A) Floating point FPGA Model

A 65kW PMSM is used as a test drive with the specifications shown in Table (1). The control algorithms are implemented on a dSPACE DS1103, while the motor model and inverter are implemented on an Altera FPGA. The sampling time is 2ms for speed control and 0.2ms for other parts of the system, such current controllers and position estimators. The speed controller produces the references i^*_d and i^*_q using a PI controller. However, a torque control algorithms are used to get i_d and i_q references by using maximum torque per ampere and flux weakening. MTPA algorithm controls the current when the speed is below the base speed, and FW controls the currents when the speed is above the base speed. The FPGA model design and the codes are shown in Fig. (6).

Table (1) PMAM parameters

P	4	R_s	0.0039655□
L_d	0.099 mH	DC-link	150v
L_q	0. 255 mH	□m	0.0427wb
J	0.0417736 kg.m^2	T_s	0.0002s
SPD_max	6000 rpm	T_{max}	134Nm

(B) dSPACE Model

dSPACE DS1103 is used to implement the modeling of the controllers and the PWM switching. The model consists of two blocks, one for DS1103 board timer interrupt with a 5□s time interrupt and includes the I/O subsystem, hence the two analogue stator currents (i_a and i_b) as well as the digital rotor position are feedback. From the motor model of FPGA, the analogue currents are converted into digital using inherent ADC Chips of dSPACE. The second block is DS1103 slave board PWM interrupt, which contains the current PI controllers, speed PI controller and PWM with 5kHz switching frequency and 4□s is the dead time. The data were transferred through the two blocks using a task transition buffer read. Figure (7) shows the dSPACE model blocks.

7. HIL Results

Figure (8) shows the HIL simulator results when the speed is 2500 rpm. It depicts that when a load is increased then a proper selection of a PI controller should be made. The current ripple caused by the hardware system and interfacing affected the estimated angle. In Fig. (8d), the estimated angle advances the actual angle when the drive is loaded and causes an estimation error due to the unstable current signal.

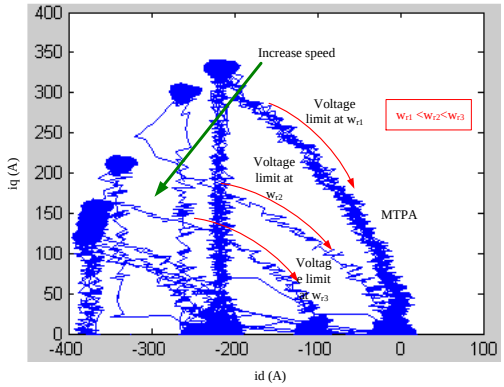

(a)

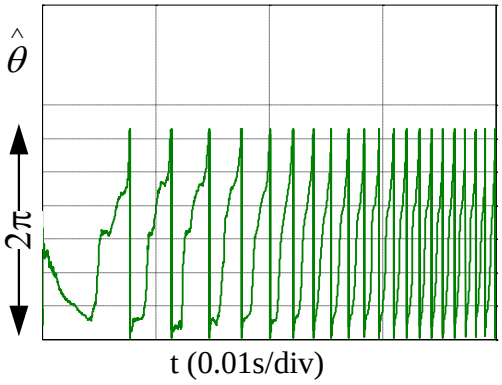

(b)

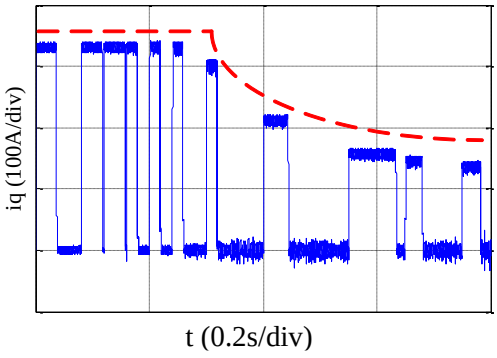

(c)

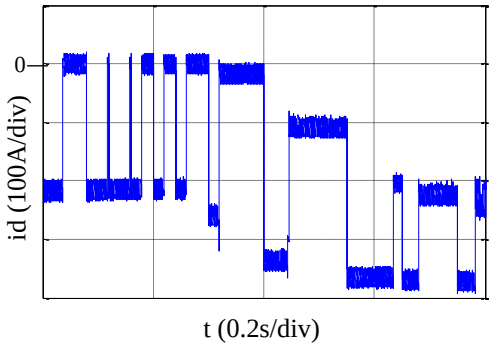

(d)

Fig. (5) MTPA & FW results including magnetic saturation effect (a) i_d-i_q loci over wide speed (b) estimated rotor position, (c) i_q ,and (d) i_d

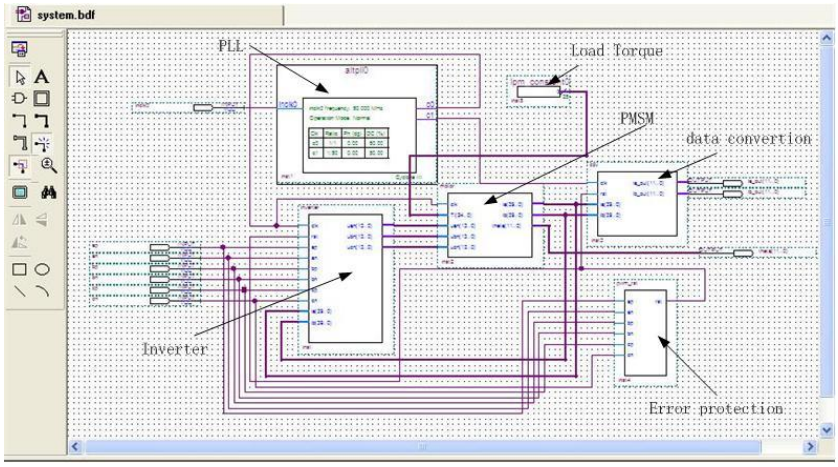

Fig. (6) FPGA design

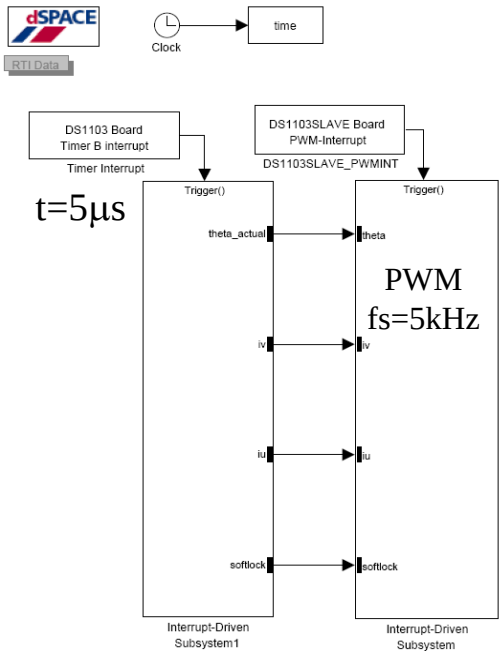

Fig. (7) dSPACE blocks model

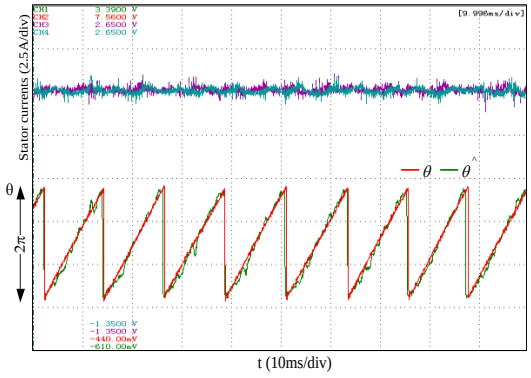

(a) no load

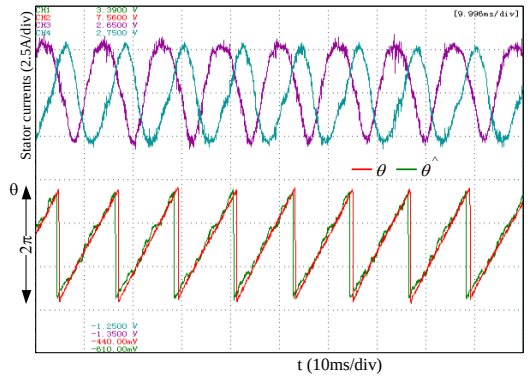

(b) loaded

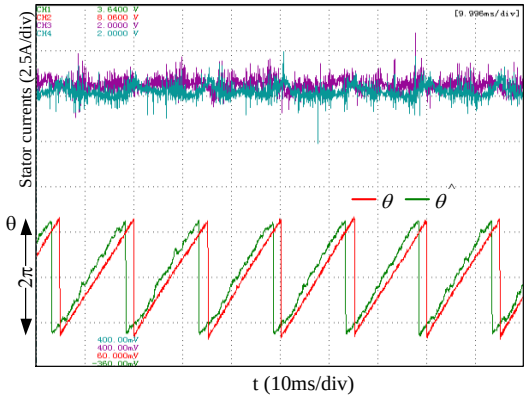

(c) no load

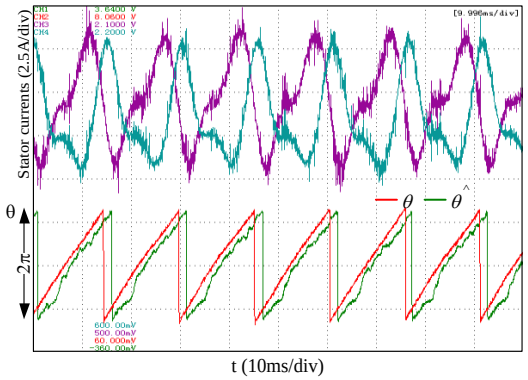

(d) loaded

Fig. (8) No load and loaded HIL Simulator sensorless results at 2500rpm without saturation (a and b) and with saturation (c and d)

8. Conclusion

A magnetic saturation effect of the sensorless control of IPMSM is investigated. Skewed slots are not considered into the finite element inductance calculation model. Sliding mode observer is used to estimate rotor position of IPMSM including the effect of cross saturation in flux weakening speed range. Cross saturation influences the sensorless estimation values when the speed is increased beyond the base speed because of the nonlinearity of the parameters. The sampling time is set it accurately though a rotor position error might be low. The saturation causes a ripple in the current signal therefore an advanced estimated angle get an error with respect to the actual angle. The experimental results showed that sensorless control with including cross saturation has a large effect under load conditions. Hardware in the

loop simulator results using FPGA verified the simulated results.

References

[1] Biachi, N. and S. Bolognani, *IEEE Trans. on Industry Appl.*, 45(4) (2009) 1249-1257.

[2] Consoli, et al., *IEEE Trans. on Industry Appl.*, 46(1) (2010) 121-129.

[3] de Kock, H.W., M.J. Kamper, and R.M. Kennel, *IEEE Trans. on Power Electron.*, 24(8) (2009) 1905-1913.

[4] de Kock, H.W., M.J. Kamper, and R.M. Kennel, *IEEE Trans. on Industrial Electron.*, 67(1) (2010) 413-419.

[5] Fu, W.N., S.L. Ho and Z. Zhang, *IEEE Trans. on Magnets*, 45(10) (2009) 4668-4671.

[6] Guglielmi, P., M. Pastorelli and A. Vagati, *IEEE Trans. on Industrial Electron.*, 53(2) (2006) 429-439.

[7] Imai, N. et al., *IEEE Trans. on Industry Appl.*, 42(5) (2006) 1193-1200.

[8] Kano, Y. et al., *IEEE Trans. on Industry Appl.*, 45(4) (2009) 1325-1333.

[9] Komatsuzaki, A. and I. Miki, A position sensorless drive technique for switched reluctance motor with consideration of magnetic saturation at low and medium speeds, Industry Applications Conf., 2006, 41st IAS Annual Meeting, pp. 1995-2000.

[10] Hasan, S.M.N., I. Husain and A. Leuenberger, IEEE Trans. on Industry Appl., 45(2) (2009) 772-781.

[11] Han, Y.S., J.S. Choi and Y.S. Kim, *IEEE Trans. on Magnetics*, 36(5) (2000) 3588-3591.

[12] Dawood, H.M. and H. Surong, Sensorless control approach based adaptive fuzzy logic controller for IPMSM drive with an online stator resistance estimation, in 2009 Pacific-Asia Conf. on Knowledge Engineering and Software Engineering (KESE2009), 2009, Shenzhen-China, pp. 220-223.

[13] Reigosa, D.D. et al., *IEEE Trans. on Industry Appl.*, 46(6) (2010) 2467-2474.

